# Apolipoprotein E is a novel marker for chondrocytes in the growth plate resting zone

Satoru Otsuru

SOtsuru@som.umaryland.edu

University of Maryland, Baltimore    https://orcid.org/0000-0002-9233-6614

**Joe Kodama**

University of Maryland    https://orcid.org/0000-0001-8331-7772

**Takeshi Oichi**

University of Maryland, Baltimore    https://orcid.org/0000-0002-8009-1648

**Kevin Wilkinson**

University of Maryland

**Joshua Abzug**

University of Maryland

**Takashi Kaito**

Osaka University

**Motomi Iwamoto-Enomoto**

University of Maryland, Baltimore    https://orcid.org/0000-0002-9589-9607

**Masahiro Iwamoto**

unknown

---

**Additional Declarations:** (Not answered)

---

# Abstract

The resting zone (RZ) in mammalian growth plates is critical for maintaining and regulating chondrocyte turnover during longitudinal bone growth as a control tower and stem cell reservoir. Although recent lineage tracing studies have identified several markers for stem cells in the RZ, these markers only partially label chondrocytes in the RZ, suggesting that the resting chondrocytes (RCs) are a heterogeneous population with different types of stem cells. Since a comprehensive marker for RCs is still lacking, the RZ is generally determined based on ambiguous histological criteria, such as small and round chondrocytes without columnar formation, which may lead to inconsistencies among researchers. Therefore, in this study, we used single-cell RNA sequencing (scRNAseq) of growth plate chondrocytes followed by validation by fluorescence in situ hybridization (FISH) to precisely annotate cell clusters in scRNAseq and search for a marker of RCs. The scRNAseq analysis revealed that apolipoprotein E (*Apoe*) was the top-hit gene, which was ubiquitously expressed in the RC cluster. FISH confirmed that *Apoe* was exclusively localized to the histologically defined RZ. In newly generated Apoe-mCherry knock-in mice, we further confirmed that mCherry expression mirrored the distribution of *Apoe*-expressing chondrocytes in the RZ particularly after the formation of the secondary ossification center. These mCherry[+] RCs were slow cycling *in vivo* and exhibited stem cell properties both *in vitro* and *in vivo*. Moreover, APOE was detected in human growth plate RCs. These findings suggest that Apoe is a novel pan-RC marker in both mouse and human growth plates.

# Introduction

Postnatal longitudinal bone growth occurs by explosive endochondral bone formation in the cartilaginous growth plates located at both ends of long bones between the epiphysis and metaphysis. Histologically, despite the high cell turnover, the growth plate is well-organized and stratified into a resting zone (RZ), proliferative zone (PZ), prehypertrophic zone (PHZ), and hypertrophic zone (HZ). The RZ, which contains round resting chondrocytes (RCs), is situated at the top of the growth plate, closest to the secondary ossification center (SOC). The RCs then give rise to flattened amplifying chondrocytes, which stack in columns in the PZ. Subsequently, the chondrocytes exit the cell cycle and accumulate matrices in the PHZ. The cells then increase in size to become mature hypertrophic chondrocytes and undergo calcification in the HZ. Eventually, these terminally differentiated hypertrophic chondrocytes undergo apoptosis or transdifferentiation into osteoblasts[1−3], exit the growth plate, and the remaining calcified cartilage is replaced by bone[4,5]. This rapid and continuous turnover of the growth plate chondrocytes must be precisely regulated, especially during the growth spurt[6−8].

In mice, after SOC formation, the RZ harbors skeletal stem cells that undergo self-renewal and asymmetric cell division to continuously supply chondrocytes to form columns in the proliferative zone[9]. In addition to being a cellular reservoir, the RZ also plays a regulatory role in chondrocyte proliferation and maturation by secreting paracrine factors such as PTHrP[10]. Moreover, in the vicinity of the

vascularized SOC, the RCs act as sensors of systemic hormonal and nutrient signals that regulate linear growth[6,8].

However, to date, there is no fully accepted criterion for histologically defining the RZ and/or RCs. As a result, most of the studies investigating the RZ in growth plates use ambiguous definitions of RCs based on their cell shape, making it difficult to accurately separate the RZ from the PZ without interpersonal bias. Recent studies have identified several markers that label stem cells in the RZ, such as *Pthlh*[11], *Axin2*[12,13], and *Foxa2*[14]. Lineage tracing of stem cells expressing these markers has successfully demonstrated that these stem cells can form columns in the growth plate. However, none of these markers could completely label all RCs or all the columns in the entire growth plate, suggesting that RCs are heterogeneous populations and that these markers may label subsets of RCs. Therefore, we sought to identify pan-RC markers that are commonly but specifically expressed in RCs by transcriptomic analysis of growth plate chondrocytes.

Single-cell RNA sequencing (scRNAseq) has become widely available. It is becoming indispensable to transcriptionally characterize cell populations at a single-cell resolution and to investigate the molecular mechanisms of disease. However, scRNAseq transcriptomics loses the spatial information of the cells during tissue digestion to prepare single-cell suspensions, which can make it difficult to characterize cells of interest identified histologically. On the other hand, spatial transcriptomics of hard tissues is still technically challenging and single-cell resolution has not been achieved[15,16]. Therefore, in this study, we utilized RNA fluorescence in-situ hybridization (FISH, RNAscope) with comprehensive gene panels on mouse growth plate tissues to spatially identify and accurately annotate the cell clusters identified by scRNAseq analysis of growth plate chondrocytes. This approach allowed us to distinguish RCs from other cell types and identify transcriptomes that specifically characterize RC.

# Results

### scRNAseq analysis and FISH validation precisely identified clusters of the growth plate chondrocytes.

To perform scRNAseq of growth plate chondrocytes, we harvested femora and tibiae from a female C57BL/6 mouse at 4 weeks of age during the growth spurt and removed as much soft tissue as possible under a stereomicroscope. The distal femoral epiphysis and proximal tibial epiphysis were then dislodged at the growth plate and the metaphysis was dissected out (Fig. S1a). The dislodged epiphysis and dissected metaphysis were digested to isolate growth plate chondrocytes. Hematopoietic cells and red blood cells were removed by magnetic beads for CD45 and Ter119 antibodies, and the resulting single-cell suspension was subjected to scRNAseq on the 10x Genomics platform. Unsupervised data analysis using the Seurat package provided a uniform manifold approximation and projection (UMAP) with 11 distinct cell clusters based on their gene expression profiles (Fig. 1a). Based on the characteristics of the transcriptomes, these 11 clusters appeared to contain not only chondrocytes, but also other cell types such as osteoblasts, endothelial cells, ligamentous fibroblasts, and mesenchymal progenitor cells (Fig. 1b). To annotate the clusters with the goal of distinguishing growth plate

chondrocytes from other cell types, we examined gene expression of marker genes that have been reported to be expressed in a specific cell type, followed by histologic validation by FISH on histological sections of 4-week old mice. Aggrecan (*Acan*) is a pan marker for chondrogenic cells, including articular chondrocytes (Fig. [1]c-1, 1c-2), growth plate chondrocytes (Fig. [1]c-1, 1c-3), and, at a lower expression level, perichondral cells (Fig. [1]c-1, 1c-4). To distinguish articular chondrocytes from growth plate chondrocytes, we used *Prg4* (proteoglycan 4 or lubricin)[17–19] and *Epyc* (epiphycan)[20,21]. *Prg4* is highly expressed in articular chondrocytes and meniscal cells (Fig. [1]d-1, 1d-2) as well as in ligament cells (Fig. 1d-3), but its expression in growth plate chondrocytes and perichondrial cells is minimal (Fig. 1d-4), consistent with a previous report[22]. In contrast, *Epyc* is specifically expressed in growth plate chondrocytes (Fig. [1]e-1, 1e-3) but not in articular chondrocytes (Fig. 1e-2) or perichondrial cells (Fig. 1e-4). Perichondrial cells specifically express *Postn* (periostin) (Fig. 1f). They also express relatively low levels of *Acan*, but higher levels of *Col1a1* compared to chondrocytes (Fig. 1g). Notably, they can be distinguished from *Col1a1*-expressing osteoblasts, which are mainly located in the trabecular and endosteal areas, because they do not express *Bglap*, a marker for mature osteoblasts[23]. Consistent with previous reports, a fraction of perichondral/periosteal cells in the outer layer express *Ctsk*[24–26], although to a lesser extent compared to osteoclasts in the trabecular area (Fig. 1h). We also identified a cluster of cells expressing *Lepr* and *Pdgfrb*, two markers of bone marrow mesenchymal progenitor cells (MPCs)[27–29]. FISH confirmed that *Lepr*[+]*Pdgfrb*[+] MPCs were mainly located in the trabecular region and not in the growth plate (Fig. 1i). In addition, we observed that these two markers, especially *Pdgfrb*, are robustly expressed in the perichondrium and periosteum (Fig. 1i), which is consistent with previous observations[28,29]. With this scRNAseq analysis and FISH validation approach, we were able to annotate the 11 clusters with 5 clusters of growth plate chondrocytes (GP1-5, *Acan*[high]*Epyc*[+]*Prg4*^{–}), articular chondrocytes (AC, *Acan*[high]*Prg4*^{+}), perichondrial cells (PeriChon, *Postn*[+]*Acan*[low]*Col1a1*[+]*Bglap*[–]*Ctsk*[+]*Pdgfrb*[+]), ligamentous fibroblasts (LF, *Eln*[+]*Fn1*^{+}*Prg4*^{+}), osteoblasts (OB, *Col1a1*[+]*Bglap*[+]), mesenchymal progenitor cells (MPCs, *Pdgfrb*[+]*Lepr*[+]), and endothelial cells (EC, *Pecam1*^{+}*Emcn*[+]) (Fig. 1b).

### Apoe is ubiquitously and specifically expressed in growth plate RCs.

To further analyze growth plate chondrocytes, clusters containing growth plate chondrocytes in Fig. 1a (GP1-5) were selected and re-clustered. The transcriptomic profiles of chondrocytes in different zones within the growth plate were analyzed and the clusters were annotated in a similar approach as in Fig. 1 (Fig. 2a, 2b). FISH confirmed the spatial gene expression of genes representing chondrocytes in each zone. For each gene, we compared the localization in tissue sections with our scRNAseq UMAP side-by-side to validate our annotation (Fig. 2c). *Clu* (Clusterin)[30] and *Pthlh* (PTHrP)[11], two previously reported markers for RCs, were specifically expressed in subsets of RCs in the upper layer of the growth plate (Fig. 2c, RC. Enlarged images for *Pthlh* are shown in Fig.S2a). *Ccnd1* (Cyclin D1), which modulates the transition from G1 to S phase[31], was mainly expressed at the boundary between unorganized RCs and

column-forming proliferating chondrocytes (Fig. 2c, Mito-C, top), suggesting that *Ccnd1* labels chondrocytes entering the cell cycle from the quiescent state. On the other hand, the mitotic gene *Mki67*, which is maximally expressed in the G2 and M phases[32], was specifically expressed in a cluster in the UMAP, but these *Mki67*-expressing chondrocytes were sparsely distributed in the proliferative zone (Fig. 2c, Mito-C, bottom). *C1qtnf3* (CTRP3) was previously identified to be expressed in proliferating chondrocytes in the growth plate[33]. Consistently, we confirmed that *C1qtnf3* was specifically expressed in the columnar chondrocytes such as proliferative and prehypertrophic chondrocytes (Fig. 2c, PC, top). In addition, glucose metabolism is an essential metabolic pathway in growth plate chondrocytes[34–36]. *Pgk1*, encoding phosphoglycerate kinase 1, an essential glycolytic enzyme, was found exclusively expressed in columnar chondrocytes (Fig. 2c, PC, bottom). Finally, *Ihh* (Indian hedgehog) and *Col10a1* (Type X collagen) are robustly expressed in the prehypertrophic and hypertrophic chondrocytes, respectively (Fig. 2c, PHC/HC). Therefore, we annotated the clusters as shown in Fig. 2a. Pseudotime analysis of these five clusters also showed that the pseudotime score increased as chondrocytes shifted from RC to HC in the UMAP, which also supports our cluster annotation (Fig. 2d). After identifying the cluster for RCs, we searched for marker genes that were ubiquitously expressed in RCs (minimum percentage of expressing cells in the cluster > 90%) and specifically expressed in RCs (the minimum fold change compared to the other four clusters; logFC > 1). Among the 41 differentially expressed genes meeting these criteria, apolipoprotein E (*Apoe*) had the highest fold change (logFC = 3.87) and was expressed in the majority of cells in the RC cluster (> 99%) (Fig. 2e). FISH combined with *Apoe*, *C1qtnf3*, and *Col10a1*, confirmed that *Apoe* was ubiquitously and specifically expressed in the resting zone separated from the PZ/PHZ (*C1qtnf3*⁺) and HZ (*Col10a1*⁺) (Fig. 2f, Fig.S2b). Immunofluorescence staining with the APOE antibody revealed that APOE was expressed in chondrocytes in the RZ but not in the PZ of the human growth plate, suggesting that apolipoprotein E may be commonly expressed in RCs across species (Fig. 2g).

# Apoe-mCherry labels RCs after the formation of the secondary ossification center

To further characterize the *Apoe*-expressing RCs, we generated Apoe-mCherry reporter mice that express mCherry protein under the control of the endogenous *Apoe* gene promoter and enhancers (the mCherry-BGHpA vector was inserted after the endogenous ATG start codon in exon 2 of the mouse *Apoe* gene) (Fig. S3a). This reporter model allows us to visualize the real-time *Apoe* expression in cells with mCherry to characterize Apoe⁺ growth plate chondrocytes *in vivo* and *in vitro*. First, colocalization of mCherry protein and *Apoe* mRNA was confirmed by a combination of immunofluorescence and FISH (Fig. S3b), indicating that mCherry expression is concomitant with endogenous *Apoe* expression. During postnatal skeletal development, mCherry expression was not detected in tibial epiphyseal cartilage at postnatal day 5 (P5), before SOC formation (Fig. 3a). mCherry-expressing chondrocytes began to appear in the tibial RZ after SOC formation at P11 (Fig. 3b). At 4 weeks of age (P28), mCherry⁺ chondrocytes lined up in the RZ, but were not detected in other zones or in articular cartilage, while some expression

was observed in the outer layer of the perichondrium (Fig. 3c. the green, yellow, and blue boxes indicate the growth plate, the articular chondrocytes, and the perichondrium, respectively). In later stages of life, the number of mCherry[+] RCs decreases over time (Fig. 3d-g), suggesting that RCs in the growth plate are exhausted after skeletal maturity with aging although some mCherry[+] RCs remain in the growth plate at 1 year of age.

## mCherry [+] RCs are slow-cycling chondrocytes.

In contrast to proliferating columnar chondrocytes, "resting" chondrocytes are quiescent with a longer cell cycle[37]. To determine whether mCherry[+] chondrocytes are slow-cycling, we performed an EdU pulse-chase assay. Specifically, we injected EdU into 2-week-old Apoe-mCherry mice for 8 consecutive days and tracked EdU incorporation into growth plate chondrocytes at 1 day, 4 days, and 14 days after the last injection (Fig. 4a). At this growing age, chondrocytes can pass through the growth plate within a few days[16]. Thus, fast-cycling cells lose the EdU label in a few days after multiple cell divisions, while slow-cycling cells can retain it. One day after the 8-day injections, approximately 60% of proliferative chondrocytes (mCherry[−]) incorporated EdU, while only 30% of mCherry[+] RC had EdU, suggesting that fewer mCherry + RCs entered the cell cycle during the 8 days compared to proliferative chondrocytes. Furthermore, as expected, proliferating columnar cells rapidly lost their EdU labeling down to ~ 30% by day 4 and ~ 6% by day 14 (Fig. 4b-c). In contrast, mCherry + cells took much longer to lose their EdU labeling (~ 30% at day 1, ~ 15% at day 4, and ~ 22% at day 14) (Fig. 4b-c), indicating that mCherry + RCs are slow-cycling compared to proliferative chondrocytes. The slight increase in EdU-positive cells in mCherry + RCs from day 4 to day 14 may be due to cell division of slow cycling RCs within the two-week window, as we observed some EdU-positive nuclei aligning close to each other, suggesting that they have just divided from a single nucleus (Fig. 4c, white arrowheads). These results suggest that our Apoe-mCherry reporter mice temporally and spatially label RCs in the growth plate.

## Apoe-mCherry RCs contain self-renewing skeletal stem cells.

After SOC formation, the RZ in the growth plate has been shown to harbor skeletal stem cells that express *Pthlh*[11], *Axin2*[12,13], or *Foxa2*[14]. These skeletal stem cells supply chondrocytes that form columns in the growth plate during linear bone growth. We found that most of the *Pthlh*-expressing stem cells expressed mCherry (Fig. 5a, ~ 94%), but only ~ 27% of the mCherry-expressing cells were *Pthlh* positive (Fig. 5a). On the other hand, the percentages of *Axin2*-expressing cells and *Foxa2*-expressing cells within mCherry + cells are 4% and 12%, respectively (Fig. S4a), which are much lower than *Pthlh*^{+} cells. To gain a holistic understanding of these stem cell populations, we examined the positivity of *Apoe*, *Pthlh*, *Axin2*, and *Foxa2* gene expression in the RC cluster of our scRNAseq dataset shown in Fig. 2a. We considered positive cells when the raw count for each gene was greater than 0. Fig.S4b shows that most RCs (> 99%) are *Apoe*[+], while *Pthlh*[+], *Axin2*^{+}, and *Foxa2*^{+} cells represent small subsets of RCs, 18%, 2%, and 4%, respectively. These percentages were slightly lower than what we observed in histology (Fig. 5a, Fig.S4a), possibly due to the different detection sensitivities between RNA sequencing and FISH.

However, the proportion of these percentages among *Pthlh⁺*, *Axin2⁺*, and *Foxa2⁺* cells is similar between scRNAseq analysis and FISH (18%, 2%, 4% in scRNAseq data, 27%, 4%, 12% in FISH, respectively). Interestingly, in these subsets of RCs, over 90% of the cells express only one of *Pthlh*, *Axin2*, or *Foxa2*, and there were no triple positive (*Pthlh⁺Axin2⁺Foxa2⁺*) cells in the RCs (Fig. S4b), suggesting that these genes label independent subsets of RCs and that skeletal stem cells in RCs are heterogeneous. Importantly, Apoe positivity in these subsets of *Pthlh⁺*, *Axin2⁺*, and *Foxa2⁺* RCs is 99%, 100%, and 97%, respectively. These results suggest that Apoe is a common marker that spans the heterogeneous subsets of skeletal stem cells in RCs.

Previous studies have identified a panel of mouse skeletal stem cell surface markers for flow cytometrical analysis[38]. We therefore examined the expression of these surface markers on mCherry⁺ RCs. Following our gating scheme to enrich singlet cells, we removed dead cells and hematopoietic/endothelial cells labeled with CD45, Tie2, and Ter119. In mCherry⁺ cells of the remaining population, we found that approximately half of the mCherry⁺ RCs were multipotent cells[38], of which ~ 18% were self-renewing mouse skeletal stem cells (SSC, CD45⁻Tie2⁻CD51⁺Thy⁻6C3⁻CD105⁻CD200⁺), ~ 29.3% were pre-bone, cartilage and stromal progenitors (pre-BCSP, CD45⁻Tie2⁻CD51⁺Thy⁻6C3⁻CD105⁻CD200⁻), and ~ 2.8% were bone, cartilage and stromal progenitors (BCSP, CD45⁻Tie2⁻CD51⁺Thy⁻6C3⁻CD105⁺) (Fig. 5b). These results demonstrated that mCherry⁺ RCs contain skeletal stem cells as well as skeletal progenitor cells, further indicating the heterogeneity of RCs.

To functionally validate that Apoe-mCherry cells contain skeletal stem cells, we sorted mCherry⁺ cells for *in vitro* and *in vivo* differentiation experiments. In addition to RCs, mCherry⁺ cells were also detected in the bone marrow (Fig. 3). Our scRNAseq analysis of bone marrow cells showed that *Apoe* was also expressed in endothelial cells, macrophages, and MPCs (data not shown). Therefore, to remove mCherry⁺ cells from the bone marrow and enrich mCherry⁺ RCs, in addition to CD31 and CD45, markers for endothelial cells and hematopoietic cells including macrophages, we utilized CD73, which has been reported as a RC marker[9]. To confirm the specificity of CD73, we separately harvested cells from the growth plate and bone marrow of Apoe-mCherry mice and examined the positivity of CD73 in mCherry⁺ cells. The majority of mCherry⁺ cells isolated from the growth plate were positive for CD73, whereas those from the bone marrow were predominantly negative (Fig. S5). Therefore, we sorted mCherry⁺ RCs as CD31⁻CD45⁻Ter119⁻CD73⁺mCherry⁺ cells and cultured them under osteogenic, chondrogenic, and adipogenic differentiation conditions (Fig. 5c). The sorted mCherry⁺ RCs were able to differentiate into osteoblasts and chondrocytes as demonstrated by alizarin red and alcian blue staining (Fig. 5c). However, these mCherry⁺ RCs exhibited limited adipogenic differentiation potential (Fig. 5c), which is consistent with previous findings regarding the non-adipogenic skeletal stem cells[38]. We then performed a colony-forming assay to determine whether mCherry⁺ RCs contain more stem cells than mCherry⁻ cells. When seeded at a low cell density (100 cells/cm²), mCherry⁺ RCs formed a significantly higher

number of colonies with cell numbers > 50 compared to mCherry⁻ cells in vitro (Fig. 5d). Finally, we transplanted mCherry⁺ RCs into kidney capsules of wild-type mice and harvested 4 weeks after the transplantation. mCherry⁺ cells formed bone nodules with the bone marrow cavity (Fig. 5e-g), demonstrating their in vivo ability to form bone and the bone marrow niche as stromal progenitors.

## Discussion

Using scRNAseq analysis and FISH validation, we identified Apoe as a novel pan-marker for RCs of postnatal mouse limb growth plates. To our knowledge, this is the first study to take advantage of FISH to intensively correlate scRNAseq results with spatial information from histological sections of growth plates. Although scRNAseq analysis is a powerful tool for dissecting the transcriptomic profiles of heterogeneous skeletal cells, the need for digestion to obtain single-cell suspensions raises several concerns, including loss of spatial information, transcriptomic changes during digestion steps, inconsistency of cell isolation, and loss of rare cell populations. These hurdles may still prevent us from fully understanding the landscape of cell composition in skeletal tissues. For example, although several recent studies using scRNAseq-based approaches have identified novel skeletal stem cell populations[38–40], we still do not know the precise locations of these skeletal stem cells in the skeleton. Emerging spatial sequencing tools such as Visium or high-plex FISH such as Nanostring and Xenium may be better alternative approaches. However, technical challenges remain for hard tissues, resolution has not yet reached the single-cell level, and/or the number of genes in a panel is limited. Our approach, combining scRNAseq and FISH validation on tissue sections, allowed us to robustly examine the locations of cells expressing genes identified from scRNAseq analysis within the growth plate tissue, leading to the identification of appropriate cell clusters to be analyzed for comprehensive characterization (Fig. 2c, f).

Previously, laser capture microdissection has been employed to profile the transcriptomes of chondrocytes in different zones of the growth plate. When the resting zone was microdissected from the proximal tibial epiphyses of 1-week or 10-day-old rats, followed by microarray analysis, more than 40 genes were identified whose expression was significantly higher in chondrocytes in the RZ than in those in other zones[15,41]. However, Apoe was not on the list, presumably because SOC formation was not complete at the age studied. On the other hand, when the transcriptomic profiles of RCs were compared between mice at postnatal day 2 and day 28, Apoe was one of the genes that were significantly upregulated at day 28, whereas its expression was minimal at day 2[9]. These previous findings are consistent with our results that RCs begin to express Apoe after SOC formation.

Several different genes have been used to mark stem cells in the RZ, such as *Pthlh*, *Axin2*, and *Foxa2*[11–14]. Lineage tracing studies of these genes have demonstrated that stem cells expressing these genes can form columns in the growth plate during longitudinal bone growth. There may be a single type of stem cell in the RZ, and these genes may mark the same stem cells at different stages of development or differentiation. However, the lineage tracing studies found that none of these genes can label the

entire growth plate columns or the entire RCs, suggesting that the RCs are heterogeneous and that there may be other stem cell populations in the RZ. Indeed, as shown in Fig. S3, our scRNAseq analysis revealed that there was little overlap in the expression of these genes in RCs, and no cell expressed all 3 genes simultaneously, also suggesting that several different types of stem cells exist in RCs. This heterogeneity of stem cells in the RZ is further supported by some observations in previous studies. For example, the dependence of canonical Wnt signaling appears to be opposite between *Axin2*^{+} cells[12] and *Pthlh*^{+} cells[22], and *Foxa2*^{+} cells and *Pthlh*^{+} cells are geographically separated and primarily localized in the upper and lower layers of the RZ, respectively[14]. Further investigation is required to dissect the cell composition of RCs. Given that the majority of cells expressing *Pthlh*, *Axin2*, or *Foxa2* are included in mCherry[+] RCs in our Apoe-mCherry mice, this mouse model may be useful for studies to comprehensively characterize the heterogeneous RC population.

Apoe labels RCs in the growth plate after SOC formation (Fig. 3a-c). Thus, these RCs must supply chondrocytes to the growth plate during postnatal growth. Compared to the embryonic and neonatal stages before SOC formation, postnatal growth has a slower growth rate[42]. However, the total amount of growth is much greater and extends over a longer period of time. During this period, individuals are exposed to external stimuli from nutritional status, injury, and disease that can significantly affect skeletal growth. In these situations, RCs play an essential role by sensing systemic cues such as nutrient deprivation[13], modulation of growth plate activity[43], or regeneration[14]. The Apoe-mCherry mice generated in this study would be a useful tool to further characterize RCs under these conditions and to understand the mechanisms underlying skeletal growth retardation.

Interestingly, ApoE-positive cells were still present in the growth plate even at 1 year of age, although the number was remarkably reduced (Fig. 3g). In contrast to humans, mouse long bone growth plates do not close, suggesting that mouse growth plates are still equipped with the necessary cellular components, including stem cells, even after their skeletal maturity and may retain the potential to grow further if they are in the growing environment. Therefore, it would be interesting to investigate the differences between mCherry + RCs in young and old (after growth arrest) to understand the mechanism underlying growth plate inactivation during aging.

We have demonstrated that Apoe is highly and specifically expressed in RCs in both mouse and human growth plates. This conserved expression of Apoe across species may suggest that Apoe plays a biological role in the growth plate. However, it remains unknown whether Apoe expression has any biological significance. It has been reported that mice with global deletion of Apoe (Apoe KO mice) have significantly shorter nose-rump lengths compared to wild-type mice[44]. We also found that Apoe KO mice had significantly shorter femora and tibiae compared to their wild-type littermates (data not shown). These findings suggest that Apoe may not only be a marker of RCs but may also have a functional role in longitudinal bone growth. The role of Apoe in RCs is currently being investigated in our laboratory.

In conclusion, using scRNAseq analysis and the FISH validation approach, we have successfully identified Apoe as a specific and ubiquitous marker of RCs in the mouse growth plate. APOE expression

was also detected in human growth plate RCs. Using the newly generated Apoe-mCherry mice, Apoe-expressing RCs were shown to contain skeletal stem cells, consistent with RC characteristics. Therefore, Apoe is the first pan marker to label RCs and the Apoe-mCherry model would be a useful tool to further investigate RC biology and function.

# Materials and methods

## Mice

The University of Maryland School of Medicine IACUC has reviewed and approved all the mouse experiments in this study (IACUC protocol #0121007 and #00000649). C57BL/6J mice were obtained from The Jackson Laboratory (mouse #000664). Apoe-mCherry$^{+/-}$ mice were generated by injecting targeted 129/SvEv x C57BL/6 hybrid embryonic stem cells into CD-1 blastocysts at the Ingenious Targeting Laboratory (Ingenious Targeting Laboratory, USA). The resulting chimeras were mated to C57BL/6N wild-type mice to generate the F1 generation. The transgenic mice were then backcrossed to C57BL/J wild-type mice for at least 7 generations. Apoe-mCherry$^{+/-}$ mice were bred with C57BL/J wild-type to produce Apoe-mCherry$^{+/-}$ mice. Both male and female mice were used in this study and at least 3 mice per sex were used for quantification in each experiment.

## Human growth plate

Growth plate tissues were obtained from the fibula of a de-identified 14-year-old male patient during the epiphysiodesis surgery. The tissues were fixed in 2% formaldehyde for 7 days and embedded in the OCT compound. The University of Maryland IRB determined that this project met the definition of "Not Human Subject Research" (HM-HP-00079767-1).

## Single-cell RNA-seq and data analysis

Chondrocytes were isolated from the growth plate according to a previously described protocol with some modifications[22]. Briefly, after careful removal of soft tissues including the perichondrium, the epiphyses in the distal femur and proximal tibia were dislodged from the metaphyseal end at the primary spongiosa/growth plate junction. Both the epiphyseal and metaphyseal ends of the growth plate were then digested in HBSS (Ca$^-$Mg$^-$) with 2 units of Liberase TM (#5401119001, Sigma) at 37°C for 3 cycles of 30-minute incubations with agitation. We divided the digestion period into three cycles and washed the released cells with HBSS in each cycle to minimize the potential transcriptomic alterations due to prolonged digestion. Released cells were mechanically disassociated into a single-cell suspension by gently passing through an 18-gauge needle on a 10 mL syringe 5–10 times, followed by filtering through a 70-μm cell strainer. Hematopoietic cells (CD45$^+$, #103105, BioLegend) and red blood cells (Ter119$^+$, #116207, BioLegend) were excluded by magnetic beads (BLD-480071, BioLegend) using the MACS manual separator (Miltenyi Biotec). Cell numbers and viability were quantified before encapsulation into emulsion droplets in the Chromium Controller (10× Genomics). Libraries were constructed using 3' GEM Library Prep (10× Genomics). cDNA libraries were profiled on a NovaSeq6000 sequencer using 100-cycle

paired-end reads, targeting 10,000 cells per sample and 50,000 reads per cell. Data were processed using the 10× Genomics workflow. Cell Ranger (10× Genomics) was used for demultiplexing, barcode assignment, and unique molecular identifier (UMI) quantification. Downstream analysis was performed using Seurat v3. Cells with > 7,500 and < 1000 expressed genes and > 5% mitochondrial transcripts were excluded. Data were normalized using the SCTransform normalization method before principal component analysis and UMAP. Pseudotime analysis was performed using the Monocle 3 package in R.

# EdU labeling and detection

For 5-ethynyl-2'-deoxyuridine (EdU) pulse-chase experiments, 10 µg/g of EdU per mouse body weight (INV-A10044, Invitrogen) was injected peritoneally at the indicated time points. After permeabilization with 0.5% Triton X-100 (#9002-93-1, Sigma-Aldrich) in PBS for 30 min at room temperature, the Click-iT EdU Alexa Fluor 647 or Alexa Fluor 488 Imaging Kit (C10340 or C10329, Thermo Fisher) was used to detect EdU. The entire proximal tibial growth plate was used for analysis. The percentage of EdU + cells in mCherry$^+$ cells or that in mCherry$^-$ chondrocytes in the entire growth plate was measured using the Qupath[45].

# RNA in situ hybridization (RNAScope)

RNAScope was performed on tibiae as previously described[16,46]. Briefly, 2% formaldehyde-fixed, undecalcified bones were embedded in the OCT compound and the frozen blocks were sectioned at 10 µm using Kawamoto film[47]. The films were fixed with grease on glass slides with the sections facing up for downstream procedures. Endogenous peroxidase was blocked with 0.3% hydroxyperoxide, tissue permeabilization was performed by using Protease III, and RNAScope probe hybridization was performed using the RNAscope Multiplex Fluorescent V2 Assay kit according to the manufacturer's protocol (Advance Cell Diagnostics Inc., Newark, CA, USA). The following probes were used in this study: Apoe (#313271), Clu (#427891), Pthrp (#456521), Prg4 (#437661), Ctsk (#464071), Epyc (#572901), Pgk1 (#312961), Slc2a1 (#458671), Col1a1(#319371), Bglap (#478941), Lepr (#402731), Pdgfrb (#411381), Mki67 (#416771), Ccnd1 (#442671), Ihh (#413091), and Col10a1 (#467961). Stained images were captured with a BZ-X All-in-One Fluorescence Microscope (Keyence) or a CSU-W1 spinning disk confocal microscope (Nikon).

# Immunofluorescence staining

2% formaldehyde- or 4% paraformaldehyde-fixed cryo-sections were stained with primary antibodies against mCherry (1:50, INV-M11217, Invitrogen) or human APOE (1:100, A0304, ABclonal) 1 hour at room temperature. For mCherry staining, antigen retrieval was performed by 0.25% trypsin for 10 minutes at room temperature prior to reaction with the primary antibody. Sections were then incubated with anti-rat (1:200, A21434, Invitrogen) or anti-rabbit (1:200, A31572, Invitrogen) secondary antibodies for 1 hour at room temperature.

# Flow cytometry and cell sorting

Both hindlimbs were harvested from 4-week-old Apoe-mCherry$^{+/-}$ mice. Growth plate chondrocytes were harvested as described for the single-cell RNA-seq and data analysis. Single cells were stained with the following cell surface markers and subjected to flow cytometrical analysis or cell sorting using an Aurora 4 UV or an Aurora CS (Cytek Biosciences).: CD45-APC (#103112, BioLegend), CD45-BV421 (#103134, BioLegend), CD31-BV421 (#102424, BioLegend), Tie2-APC (#124010, BioLegend), Ter119-APC (#116212, BioLegend), Ter119-BV421 (#116234, BioLegend), CD73-PE/Cy7 (#127223, BioLegend), CD90.1 (#202529, BioLegend), CD90.2 (#105341, BioLegend), CD51-biotin (#104104, BioLegend), Ly-51-BV711 (#740691, BD Biosciences), CD105-PE/Cy7 (#120410, BioLegend), and CD200-APC/R700 (#565546, BD Biosciences). CD51 antibody was biotinylated and detected by streptavidin conjugated with APC/Cy7 (#405208, BioLegend). To label endothelial cells, Tie2-APC was used for SSC analysis in Fig. 5b and CD31-BV421 was used for sorting.

## In vitro cell differentiation assays and colony forming unit assay

Sorted CD73$^+$mCherry$^+$CD45$^-$CD31$^-$Ter119$^-$ chondrocytes were seeded on 96-well culture plates at a density of ~ 20000 cells/cm$^2$. Osteogenic, chondrogenic, and adipogenic differentiation were induced using StemPro Differentiation Kits (A1007201/A1007001/A1007101, ThermoFisher). Alizarin Red S staining (A5533-25G, Sigma) was performed on day 7 after osteogenic induction to assess mineralization. Alcian blue (J60122, ThermoFisher) or Oil red O (O0625-25G, Sigma) staining was performed on day 14 to assess proteoglycan synthesis and lipid droplet formation as indicators of chondrogenic and adipogenic differentiation, respectively. DMEM supplemented with 10% FBS was used as control. For the CFU-F assay, sorted cells were seeded on 6-well plates at a density of 100 cells/cm$^2$ and cultured in DMEM supplemented with 20% FBS for 7 days. Colonies were stained with crystal violet (C6158-50G, Sigma).

## Kidney capsule transplantation

Sorted CD73$^+$mCherry$^+$CD45$^-$CD31$^-$Ter119$^-$ chondrocytes were transplanted into kidney capsules of 8-10-week-old wild-type C57BL/J male mice to evaluate the in vivo differentiation ability as previously described[38]. Briefly, sorted CD73$^+$mCherry$^+$CD45$^-$CD31$^-$Ter119$^-$ chondrocytes were resuspended in Matrigel (CLS356234, Sigma) at a concentration of 10000 cells/µl. 2 µl of the cell solution was drained into the outer cylinder of a 20-gauge Surflo I.V. catheter (SR-OX2032CA, Terumo) and left at room temperature for 30 minutes. Under anesthesia, a 1 cm incision was made in the back and the retroperitoneum of wild-type mice, and the left kidney was exposed. After making a small hole in the kidney capsule, the catheter was inserted between the capsule and the renal parenchyma. The cell-containing Matrigel solution was gently ejected from the catheter with the blunted end of the Surflo needle. The retroperitoneum and the skin were closed with 5 – 0 Ethilon sutures (668G, Ethicon). Mice were caged and fed *ad libitum* for four weeks postoperatively, and the kidneys were harvested and fixed in 4% paraformaldehyde solution. Bone formation was assessed by µCT scanning by Skyscan 1172

(Bruker), and the kidneys were then embedded in frozen blocks. 5 µm thick sections were stained with Movat Pentachrome Stain Kit (Ab245884, Abcam).

# Declarations

# Conflict of interests

The authors declare no competing interest.

# Contributions

J.K. and S.O. designed the research; J.M.A provided research samples. J.K., T.O., K.J.W, and S.O. performed research; J.K., T.O., K.J.W., T.K., and S.O. analyzed data; J.K. and S.O. wrote the paper; J.M.A, T.K., M.E-I., M.I., and S.O. reviewed and edited the manuscript; J.M.A., T.K., M.I. and M.E-I. provided feedback and guidance.

# Acknowledgements

# Data availability statements:

All data are presented in this manuscript. ScRNAseq dataset will be deposited to GEO and SRA databases upon acceptance of the article. Data that are mentioned but not shown in this manuscript are available from the corresponding author upon reasonable request.

# References

1. Yang, L., Tsang, K. Y., Tang, H. C., Chan, D. & Cheah, K. S. E. Hypertrophic chondrocytes can become osteoblasts and osteocytes in endochondral bone formation. *PNAS* **111**, 12097–12102 (2014).
2. Zhou, X. *et al.* Chondrocytes transdifferentiate into osteoblasts in endochondral bone during development, postnatal growth and fracture healing in mice. *PLoS Genet* **10**, e1004820 (2014).
3. Yang, G. *et al.* Osteogenic fate of hypertrophic chondrocytes. *Cell Res* **24**, 1266–1269 (2014).

4.  Bonucci, E. *Calcification in Biological Systems*. (CRC Press, Boca Raton, 2020). doi:10.1201/9781003068396.

5.  Matsushita, Y., Ono, W. & Ono, N. Growth plate skeletal stem cells and their transition from cartilage to bone. *Bone* **136**, 115359 (2020).

6.  Nilsson, O., Marino, R., De Luca, F., Phillip, M. & Baron, J. Endocrine regulation of the growth plate. *Horm Res* **64**, 157–165 (2005).

7.  Späth, S.-S., Andrade, A. C., Chau, M. & Nilsson, O. Local regulation of growth plate cartilage. *Endocr Dev* **21**, 12–22 (2011).

8.  van der Eerden, B. C. J., Karperien, M. & Wit, J. M. Systemic and local regulation of the growth plate. *Endocr Rev* **24**, 782–801 (2003).

9.  Newton, P. T. *et al.* A radical switch in clonality reveals a stem cell niche in the epiphyseal growth plate. *Nature* **567**, 234–238 (2019).

10. Kronenberg, H. M. Developmental regulation of the growth plate. *Nature* **423**, 332–336 (2003).

11. Mizuhashi, K. *et al.* Resting zone of the growth plate houses a unique class of skeletal stem cells. *Nature* **563**, 254–258 (2018).

12. Usami, Y. *et al.* Possible Contribution of Wnt-responsive Chondroprogenitors to The Postnatal Murine Growth Plate. *J Bone Miner Res* **34**, 964–974 (2019).

13. Oichi, T. *et al.* Nutrient-regulated dynamics of chondroprogenitors in the postnatal murine growth plate. *Bone Res* **11**, 20 (2023).

14. Muruganandan, S. *et al.* A FoxA2+ long-term stem cell population is necessary for growth plate cartilage regeneration after injury. *Nat Commun* **13**, 2515 (2022).

15. Xiao, X. *et al.* Spatial transcriptomic interrogation of the murine bone marrow signaling landscape. *Bone Res* **11**, 59 (2023).

16. Scheiber, A. L. *et al.* 4PBA reduces growth deficiency in osteogenesis imperfecta by enhancing transition of hypertrophic chondrocytes to osteoblasts. *JCI Insight* **7**, e149636 (2022).

17. Jay, G. D., Tantravahi, U., Britt, D. E., Barrach, H. J. & Cha, C. J. Homology of lubricin and superficial zone protein (SZP): products of megakaryocyte stimulating factor (MSF) gene expression by human synovial fibroblasts and articular chondrocytes localized to chromosome 1q25. *J Orthop Res* **19**, 677–687 (2001).

18. Kohrs, R. T. *et al.* Tendon fascicle gliding in wild type, heterozygous, and lubricin knockout mice. *J Orthop Res* **29**, 384–389 (2011).

19. Rhee, D. K. *et al.* The secreted glycoprotein lubricin protects cartilage surfaces and inhibits synovial cell overgrowth. *J Clin Invest* **115**, 622–631 (2005).

20. Nuka, S. *et al.* Phenotypic characterization of epiphycan-deficient and epiphycan/biglycan double-deficient mice. *Osteoarthritis Cartilage* **18**, 88–96 (2010).

21. Johnson, J. *et al.* Expression and localization of PG-Lb/epiphycan during mouse development. *Dev Dyn* **216**, 499–510 (1999).

22. Hallett, S. A. *et al.* Chondrocytes in the resting zone of the growth plate are maintained in a Wnt-inhibitory environment. *Elife* **10**, e64513 (2021).

23. Price, P. A., Otsuka, A. A., Poser, J. W., Kristaponis, J. & Raman, N. Characterization of a gamma-carboxyglutamic acid-containing protein from bone. *Proc Natl Acad Sci U S A* **73**, 1447–1451 (1976).

24. Debnath, S. *et al.* Discovery of a periosteal stem cell mediating intramembranous bone formation. *Nature* **562**, 133–139 (2018).

25. Han, Y. *et al.* Lkb1 deletion in periosteal mesenchymal progenitors induces osteogenic tumors through mTORC1 activation. *J Clin Invest* **129**, 1895–1909 (2019).

26. Tsukasaki, M. *et al.* Periosteal stem cells control growth plate stem cells during postnatal skeletal growth. *Nat Commun* **13**, 4166 (2022).

27. Zhou, B. O., Yue, R., Murphy, M. M., Peyer, J. G. & Morrison, S. J. Leptin-receptor-expressing mesenchymal stromal cells represent the main source of bone formed by adult bone marrow. *Cell Stem Cell* **15**, 154–168 (2014).

28. Böhm, A.-M. *et al.* Activation of Skeletal Stem and Progenitor Cells for Bone Regeneration Is Driven by PDGFRβ Signaling. *Dev Cell* **51**, 236-254.e12 (2019).

29. Komada, Y. *et al.* Origins and properties of dental, thymic, and bone marrow mesenchymal cells and their stem cells. *PLoS One* **7**, e46436 (2012).

30. Haseeb, A. *et al.* SOX9 keeps growth plates and articular cartilage healthy by inhibiting chondrocyte dedifferentiation/osteoblastic redifferentiation. *PNAS* **118**, (2021).

31. Baldin, V., Lukas, J., Marcote, M. J., Pagano, M. & Draetta, G. Cyclin D1 is a nuclear protein required for cell cycle progression in G1. *Genes Dev* **7**, 812–821 (1993).

32. Uxa, S. *et al.* Ki-67 gene expression. *Cell Death Differ* **28**, 3357–3370 (2021).

33. Maeda, T. *et al.* Cartducin, a paralog of Acrp30/adiponectin, is induced during chondrogenic differentiation and promotes proliferation of chondrogenic precursors and chondrocytes. *J Cell Physiol* **206**, 537–544 (2006).

34. Hollander, J. M. & Zeng, L. The Emerging Role of Glucose Metabolism in Cartilage Development. *Curr Osteoporos Rep* **17**, 59–69 (2019).

35. Lee, S.-Y., Abel, E. D. & Long, F. Glucose metabolism induced by Bmp signaling is essential for murine skeletal development. *Nat Commun* **9**, 4831 (2018).

36. Stegen, S. *et al.* HIF-1α metabolically controls collagen synthesis and modification in chondrocytes. *Nature* **565**, 511–515 (2019).

37. Angelozzi, M., de Charleroy, C. R. & Lefebvre, V. EdU-Based Assay of Cell Proliferation and Stem Cell Quiescence in Skeletal Tissue Sections. *Methods Mol Biol* **2230**, 357–365 (2021).

38. Chan, C. K. F. *et al.* Identification and specification of the mouse skeletal stem cell. *Cell* **160**, 285–298 (2015).

39. Bandyopadhyay, S. *et al.* Mapping the cellular biogeography of human bone marrow niches using single-cell transcriptomics and proteomic imaging. *Cell* **187**, 3120-3140.e29 (2024).

40. Zhong, L. *et al.* Single cell transcriptomics identifies a unique adipose lineage cell population that regulates bone marrow environment. *Elife* **9**, e54695 (2020).

41. Chau, M. *et al.* Gene expression profiling reveals similarities between the spatial architectures of postnatal articular and growth plate cartilage. *PLoS One* **9**, e103061 (2014).

42. Tanner, J. M. & Davies, P. S. Clinical longitudinal standards for height and height velocity for North American children. *J Pediatr* **107**, 317–329 (1985).

43. Trompet, D. *et al.* Stimulation of skeletal stem cells in the growth plate promotes linear bone growth. *JCI Insight* **9**, e165226 (2024).

44. Massaro, D. & Massaro, G. D. Apoetm1Unc mice have impaired alveologenesis, low lung function, and rapid loss of lung function. *Am J Physiol Lung Cell Mol Physiol* **294**, L991-997 (2008).

45. Bankhead, P. *et al.* QuPath: Open source software for digital pathology image analysis. *Sci Rep* **7**, 16878 (2017).

46. Gorrell, L., Makareeva, E., Omari, S., Otsuru, S. & Leikin, S. ER, Mitochondria, and ISR Regulation by mt-HSP70 and ATF5 upon Procollagen Misfolding in Osteoblasts. *Adv Sci (Weinh)* **9**, e2201273 (2022).

47. Kawamoto, T. Use of a new adhesive film for the preparation of multi-purpose fresh-frozen sections from hard tissues, whole-animals, insects and plants. *Arch Histol Cytol* **66**, 123–143 (2003).
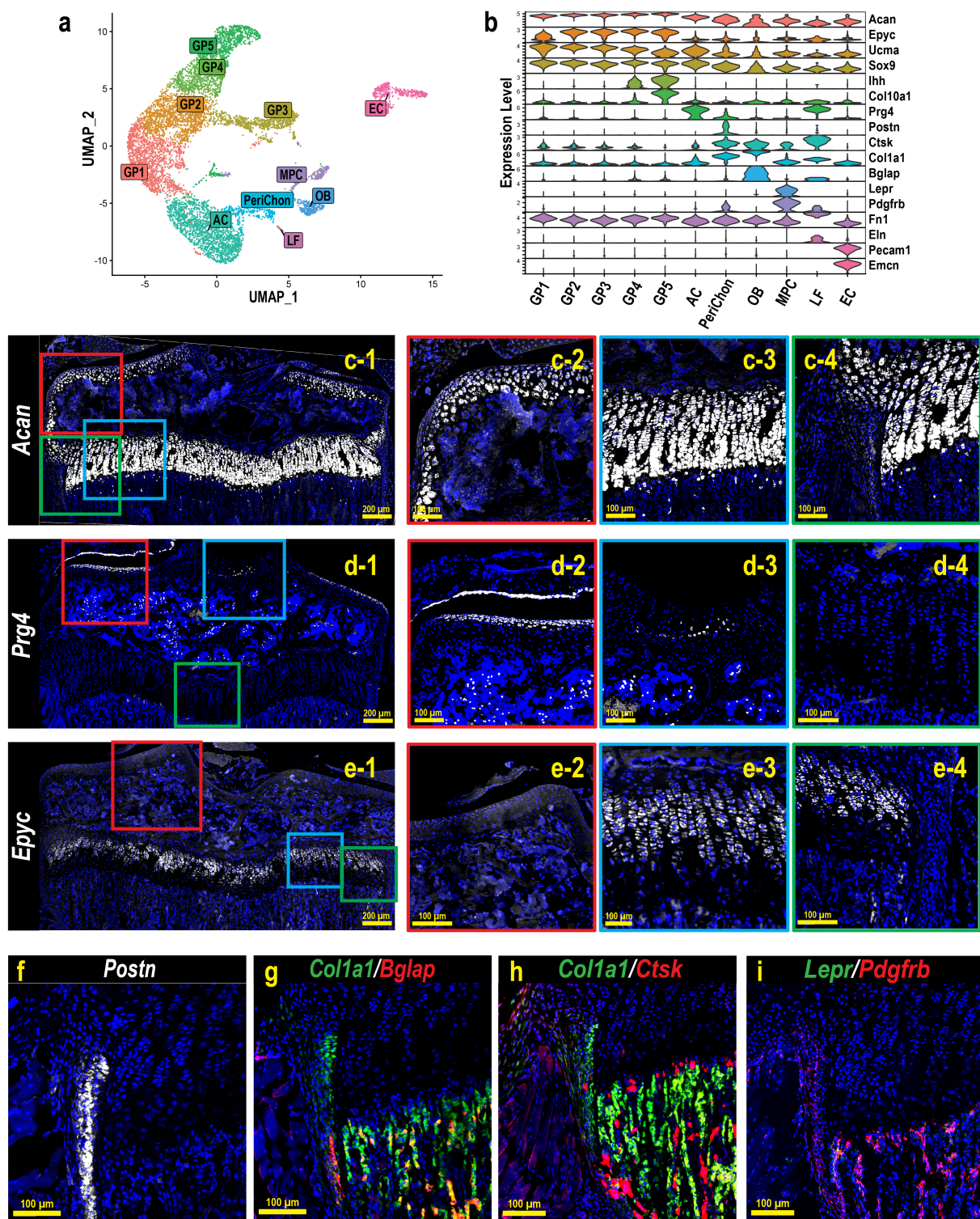
# Figures

**Figure 1**

**scRNAseq analysis and FISH validation of the single cells isolated from hindlimb growth plates.** (a) UMAP analysis of single cells obtained from the digested hindlimb epiphyseal growth plates of a 4-week-old female C57BL/6 mouse based on the transcriptomic profiles of each cell. (b) Violin plot of the gene panel selected for cluster annotation and histological validation. (c-i) FISH validations for representative genes for cluster annotation. c-2-4, d-2-4, and e-2-4 are magnified images of the corresponding colored

boxes indicated in c-1, d-1, and e-1. At least 3 mice were used for each gene and the representative images were shown.
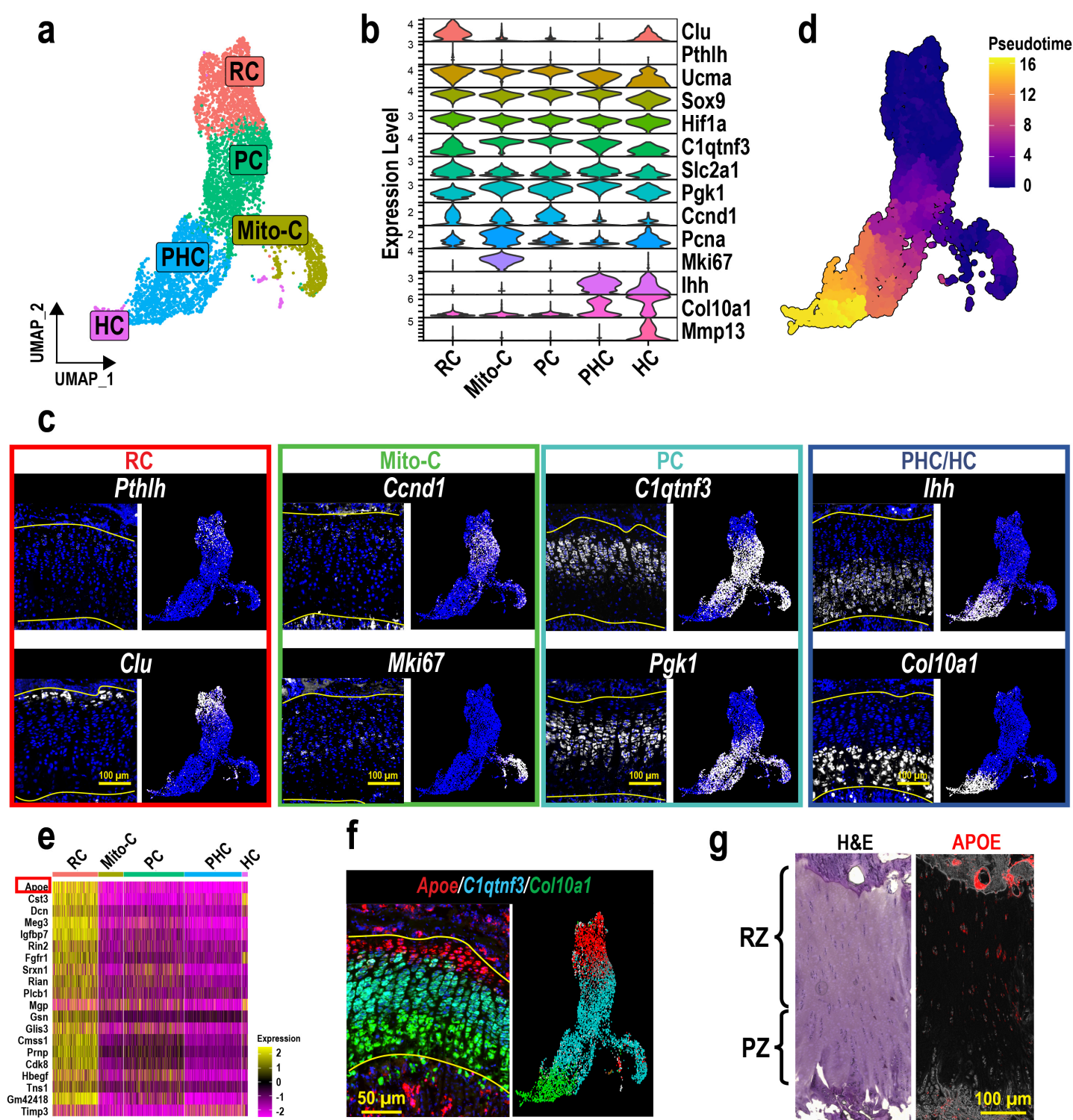


Figure 2

**Characterization of RCs by scRNAseq and FISH to identify markers for RCs.** (a) Reclustering and UMAP visualization of the GP chondrocytes selected in Fig.1a. (b) Gene panel used for cluster annotation of GP chondrocytes and FISH validation. (c) FISH images and the corresponding feature plots of genes

representing chondrocytes in different zones. (d) Pseudotime analysis of the GP chondrocytes. Higher pseudotime scores indicate more mature/differentiated chondrocytes. (e) Heatmap of the detected genes that are ubiquitously and specifically expressed in the RC cluster. (f) FISH of Apoe, C1qtnf3, and Col10a1 on a coronal section of a 4-week-old male mouse tibia. Featureplot of the three genes is shown in corresponding colors next to the FISH image. (g) Hematoxylin & Eosin (H&E) staining and immunofluorescence staining of human APOE on serial sections of human tibia. RZ: resting zone. PZ: proliferative zone. At least 3 mice were used for each gene and the representative images were shown.
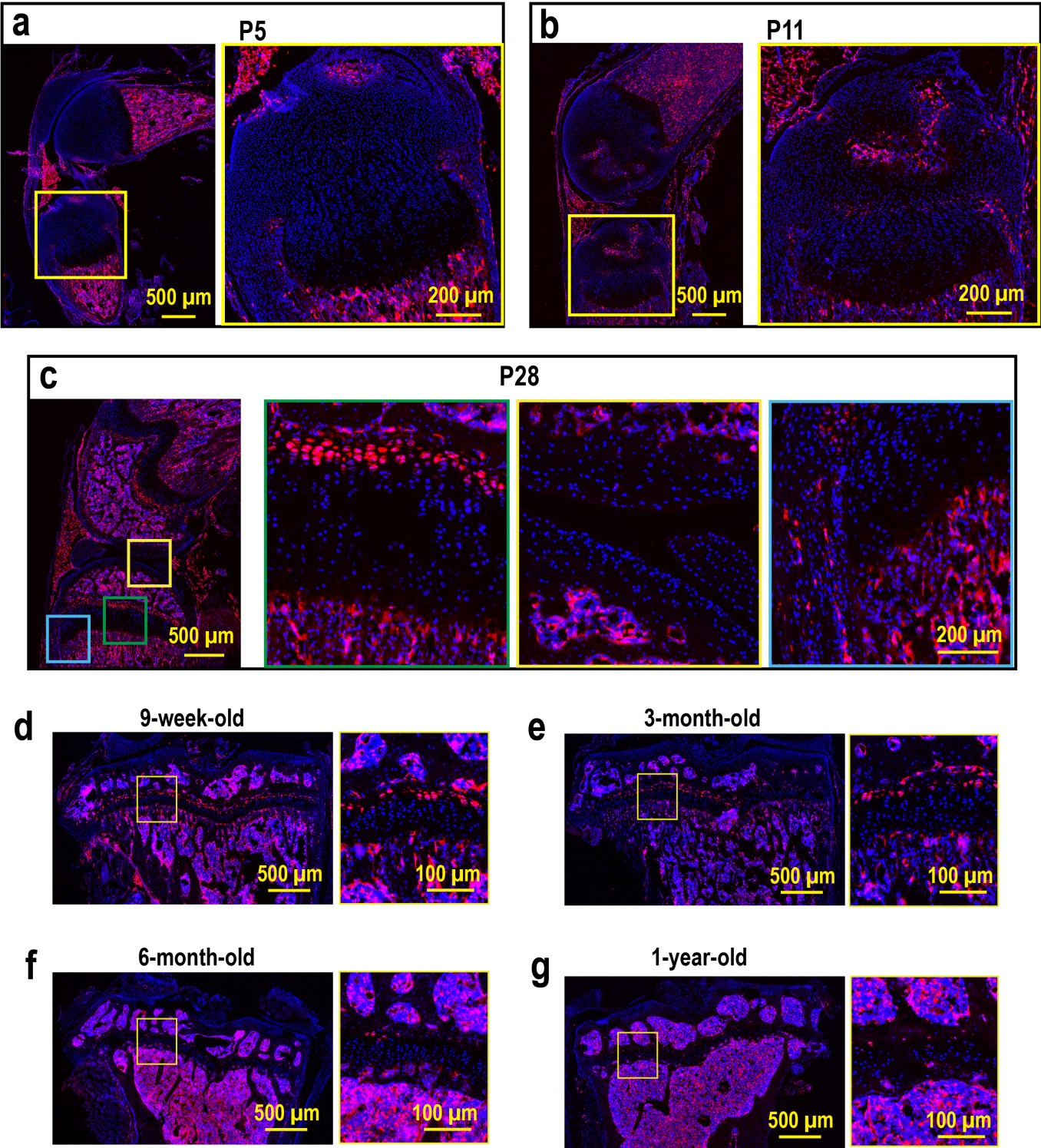
## Figure 3

**Histological analysis of Apoe-mCherry mice.** (a-c) Sagittal sections of the left knees from Apoe-mCherry$^{+/-}$ mice at postnatal day 5 (P5), day 11 (P11), and day 28 (P28, 4-week-old). (d-g) Fluorescence images of coronal sections of left tibiae from Apoe-mCherry$^{+/-}$ mice at different ages as indicated.
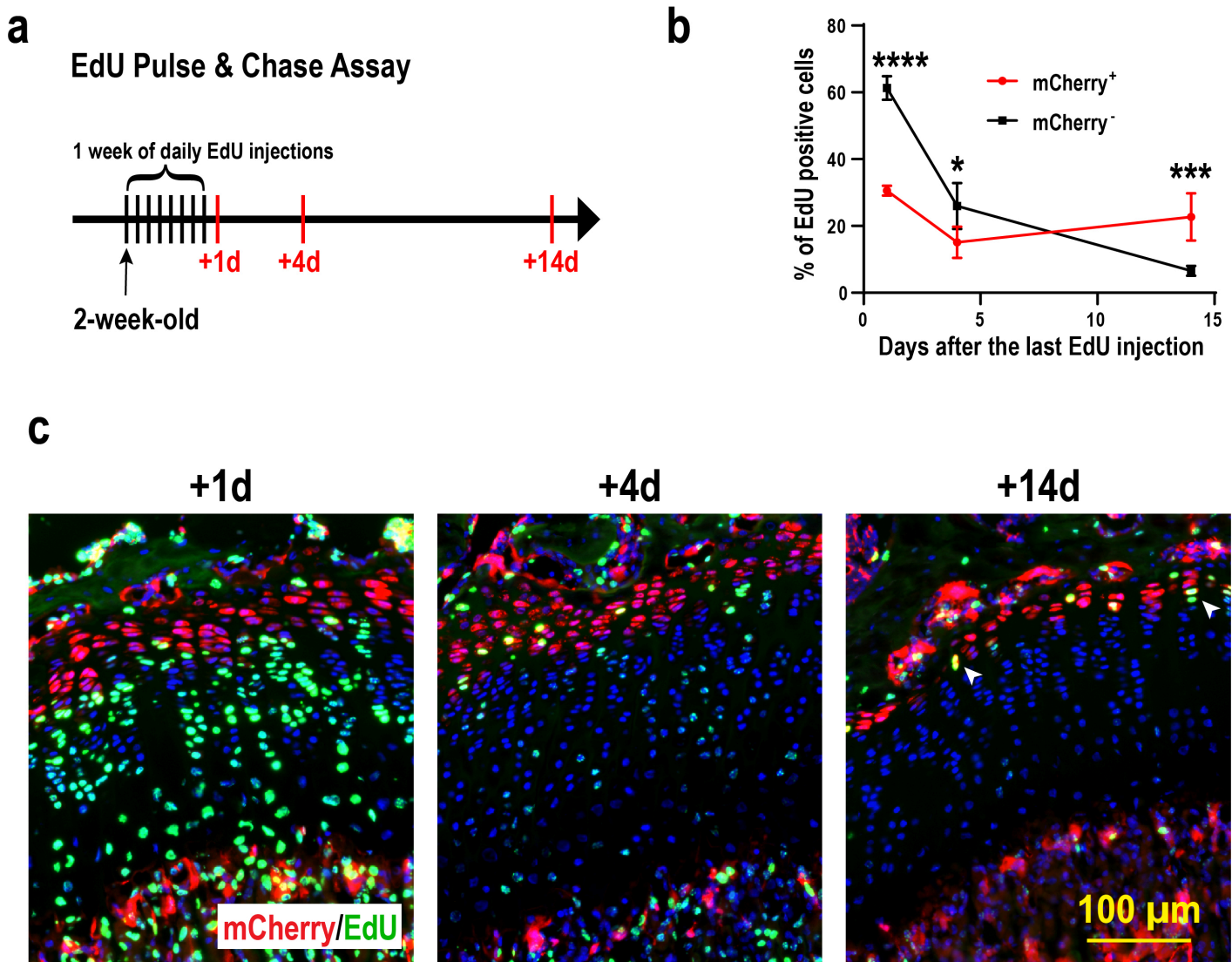


## Figure 4

**EdU pulse & chase assay in Apoe-mCherry mice.** (a) Experimental scheme of the EdU injections and sampling. 8-day EdU injection started at 2 weeks of age and tibiae were harvested 1, 4, and 14 days after the last injection. (b) Percentage of EdU+ cells in mCherry+ RCs (red) and mCherry- proliferative chondrocytes (black) at the indicated time points. Data are from male mice and presented as mean ± SD. n=3 for +1d and +4d. n=4 for +14d. *: p=0.004, ***: p=0.0003, ****: p<0.0001. Two-way ANOVA (factor mCherry: p=0.0016; factor Time: p<0.0001) followed by Tukey's multiple comparison test. (c) Representative images of EdU detection (green) and mCherry immunofluorescence (red) with DAPI

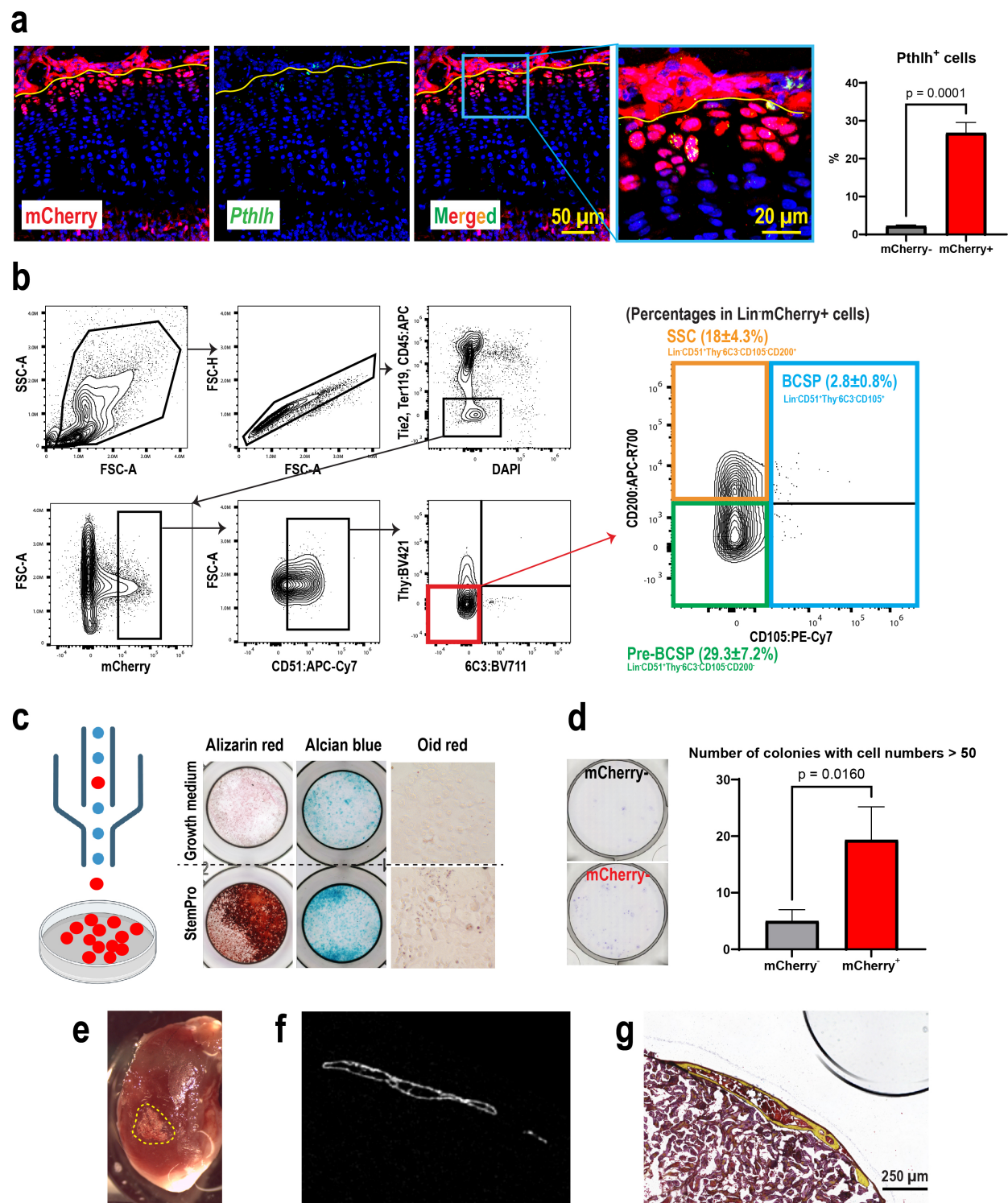(blue). White arrowheads indicate two adjacent EdU$^+$ nuclei that have presumably divided from a single nucleus.



**a**

mCherry | *Pthlh* | Merged | 50 μm | 20 μm

Pthlh$^+$ cells

p = 0.0001

mCherry-  mCherry+

**b**

(Percentages in Lin$^-$mCherry+ cells)

SSC (18±4.3%)
Lin$^-$CD51$^-$Thy$^-$6C3$^-$CD105$^-$CD200$^+$

BCSP (2.8±0.8%)
Lin$^-$CD51$^+$Thy$^-$6C3$^-$CD105$^+$

Pre-BCSP (29.3±7.2%)
Lin$^-$CD51$^+$Thy$^-$6C3$^-$CD105$^-$CD200$^-$

**c**

Alizarin red | Alcian blue | Oid red

Growth medium

StemPro

**d**

mCherry$^-$

mCherry$^-$

Number of colonies with cell numbers > 50

p = 0.0160

mCherry$^-$  mCherry$^+$

**e**  **f**  **g**

250 μm

Figure 5

**Characterization of mCherry RCs for stem cell properties.** (a) FISH for *Pthlh* to determine whether mCherry$^+$ RCs express *Pthlh* (red: mCherry, green: *Pthlh*, blue: DAPI). The percentage of *Pthlh$^+$* cells in

mCherry$^+$ RCs and mCherry$^-$ RCs was examined. (b) The gating scheme of flow cytometric analysis of GP cells isolated from 4-week-old male Apoe-mCherry$^{+/-}$ mice (n=3). Percentages are within DAPI$^-$Lin$^-$ mCherry$^+$ cells. Lin: hematopoietic and endothelial lineage cells (CD45$^+$Tie2$^+$Ter119$^+$). (c) Lin$^-$ CD73$^+$mCherry$^+$ cells were sorted and subjected to in vitro osteogenic/chondrogenic/adipogenic differentiation assays. The upper panels are controls cultured in non-differentiating media (n=3). (d) Colony forming unit (CFU) assay comparing the self-renewal capabilities between Lin$^-$CD73$^+$mCherry$^-$ and Lin$^-$CD73$^+$mCherry$^+$ cells. (e) Photographs of harvested kidneys 4 weeks after transplantation of isolated Lin$^-$CD73$^+$mCherry$^+$ cells in Matrigel. The yellow dotted area indicates the transplanted region. (f-g) Representative μCT image and histological image (Movat Pentachrome Staining) of a similar plane (n=4).

## Supplementary Files

This is a list of supplementary files associated with this preprint. Click to download.

- Kodamaetal.supplementaryfigures.docx